Cell Stem Cell, Volume *27*

Supplemental Information

Human Lung Stem Cell-Based Alveolospheres Provide Insights into SARS-CoV-2-Mediated Interferon Responses and Pneumocyte Dysfunction

Hiroaki Katsura, Vishwaraj Sontake, Aleksandra Tata, Yoshihiko Kobayashi, Caitlin E. Edwards, Brook E. Heaton, Arvind Konkimalla, Takanori Asakura, Yu Mikami, Ethan J. Fritch, Patty J. Lee, Nicholas S. Heaton, Richard C. Boucher, Scott H. Randell, Ralph S. Baric, and Purushothama Rao Tata

Figure S1

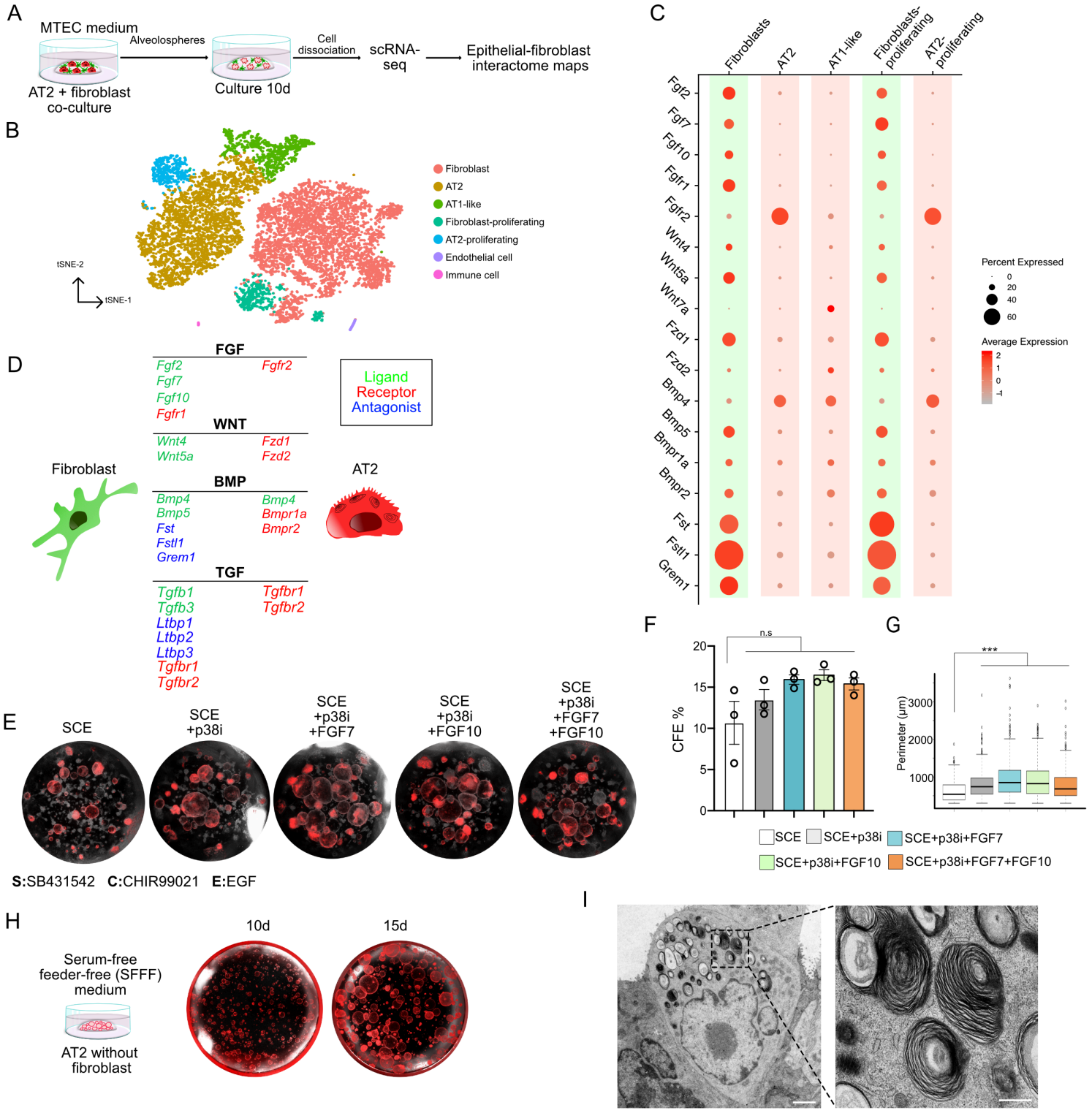

Fig. S1. Alveolar stem cell niche receptor-ligand interactome guided optimization of medium components for defined conditions for alveolosphere cultures. Related to Fig. 1. A. Schematic of the experimental design. B. t-SNE visualization of epithelial cells and fibroblasts from mouse alveolosphere culture. Cells are colored by cluster assignment based on marker genes expression. A small number of endothelial and blood cell contamination was observed. C. Dot plots showing gene expression of receptors, ligands, and regulators in key signaling pathways in each cluster. Dot size and color intensity indicate the number of cells expressing the indicated transcript and the expression level, respectively. D Schematics of the receptor-ligand interactions between AT2s and fibroblasts in alveolosphere culture. E. Representative images of alveolospheres in each culture condition. SCE refers to: SB431542, CHIR99021 and EGF. Scale bar, 1mm. F. Quantification of colony forming efficiency (CFE) in each condition. Error bars indicates mean ± s.e.m. (n = 3, at least two wells per condition). In E and F, red color indicates tdTomato expression from Sftpc-creER;R26R-tdTomato. G. alveolospheres that are greater than 300μm in perimeter were quantified in each condition. SCE vs SCE+p38i, $p=1.65x10^{-10}$; SCE vs SCE+p38i+FGF7, $p=5.47x10^{-14}$; SCE vs SCE+p38i+FGF10, $p=4.94x10^{-14}$; SCE vs SCE+p38i+FGF7_FGF10, $p=5.1x10^{-6}$; n.s, not significant; Steel-Dwass test. H. Schematic and representative images of alveolosphere cultures derived from labeled (tdTomato+) in SFFF medium. I. Representative TEM images of alveolospheres cultured in SFFF medium. Scale bar, 2 μm. Higher-magnification image (right) shows lamellar body-like structures. Scale bar, 500 nm.

Figure S2

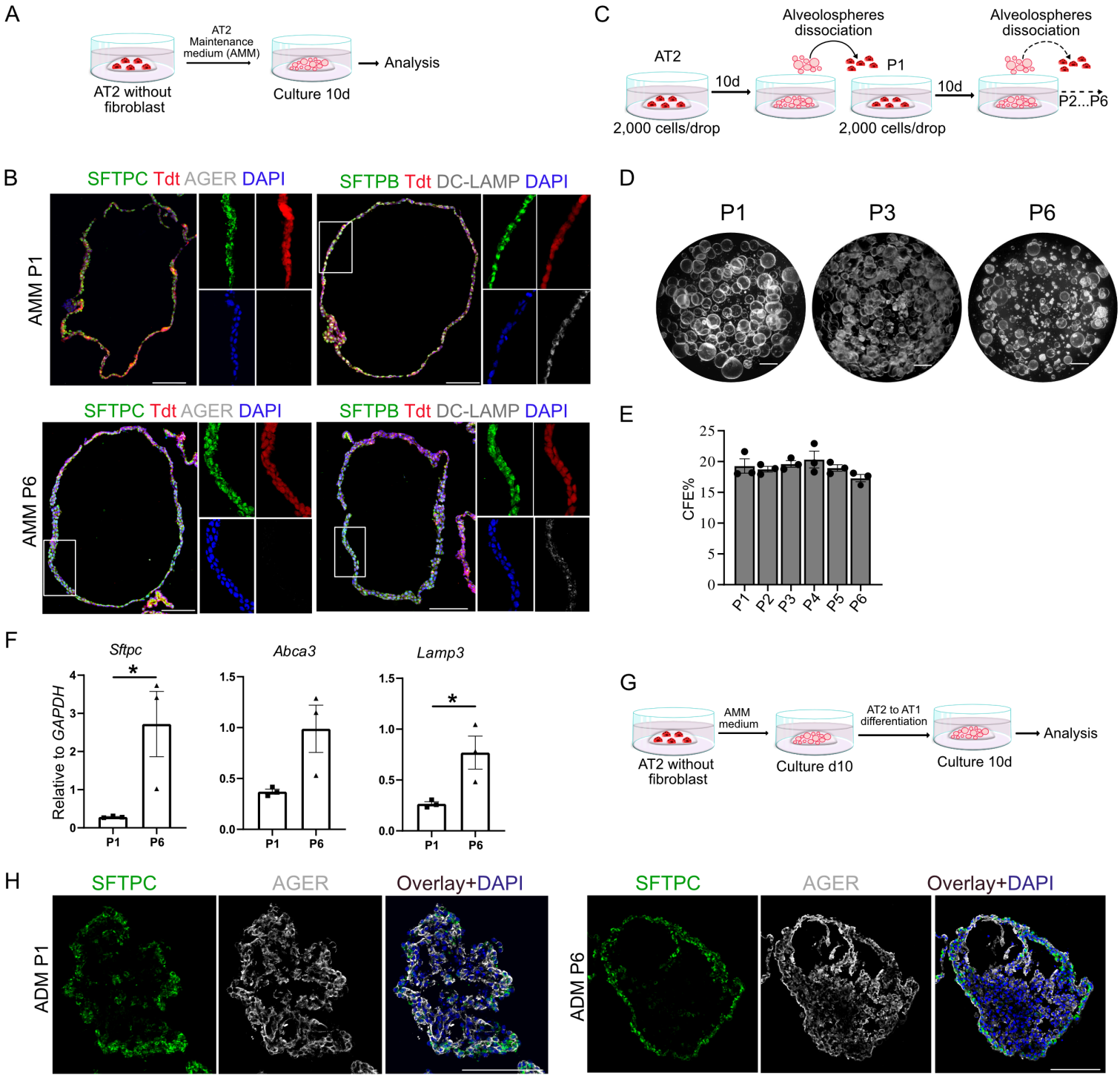

Fig. S2. Establishment of chemically defined fibroblast-free alveolosphere culture system. Related to Fig. 1.
A. Schematic representation of mouse alveolosphere cultures in AMM. B. Immunostaining for SFTPC (green), Tdt (red), and AGER (grey) (left panel) or SFTPB (green), Tdt (red) and DC-LAMP (grey) (right panel) at P1 and P6 mouse alveolospheres cultured in AMM. C. Schematic representation of mouse alveolosphere passaging. D. Representative alveolosphere images at passage 1, 3 and 6. E. Quantification of CFE at different passages. F. Quantitative RT-PCR for *Sftpc*, *Abca3* and *Lamp3* in mouse alveolospheres at P1 and P6. Asterisks show $p < 0.05$. G. Schematic representation of mouse AT2 differentiation cultures. Sorted AT2 from mouse lungs were cultured in AMM for 10 days followed by culture in ADM for 10 days. H. Immunostaining for SFTPC (green) and AGER (gray) in mouse alveolospheres cultured in ADM at P1 (left) and P6 (right). Scale bars: D, 1 mm; B and G 50 μm. Data are presented as mean s.e.m.

Figure S3

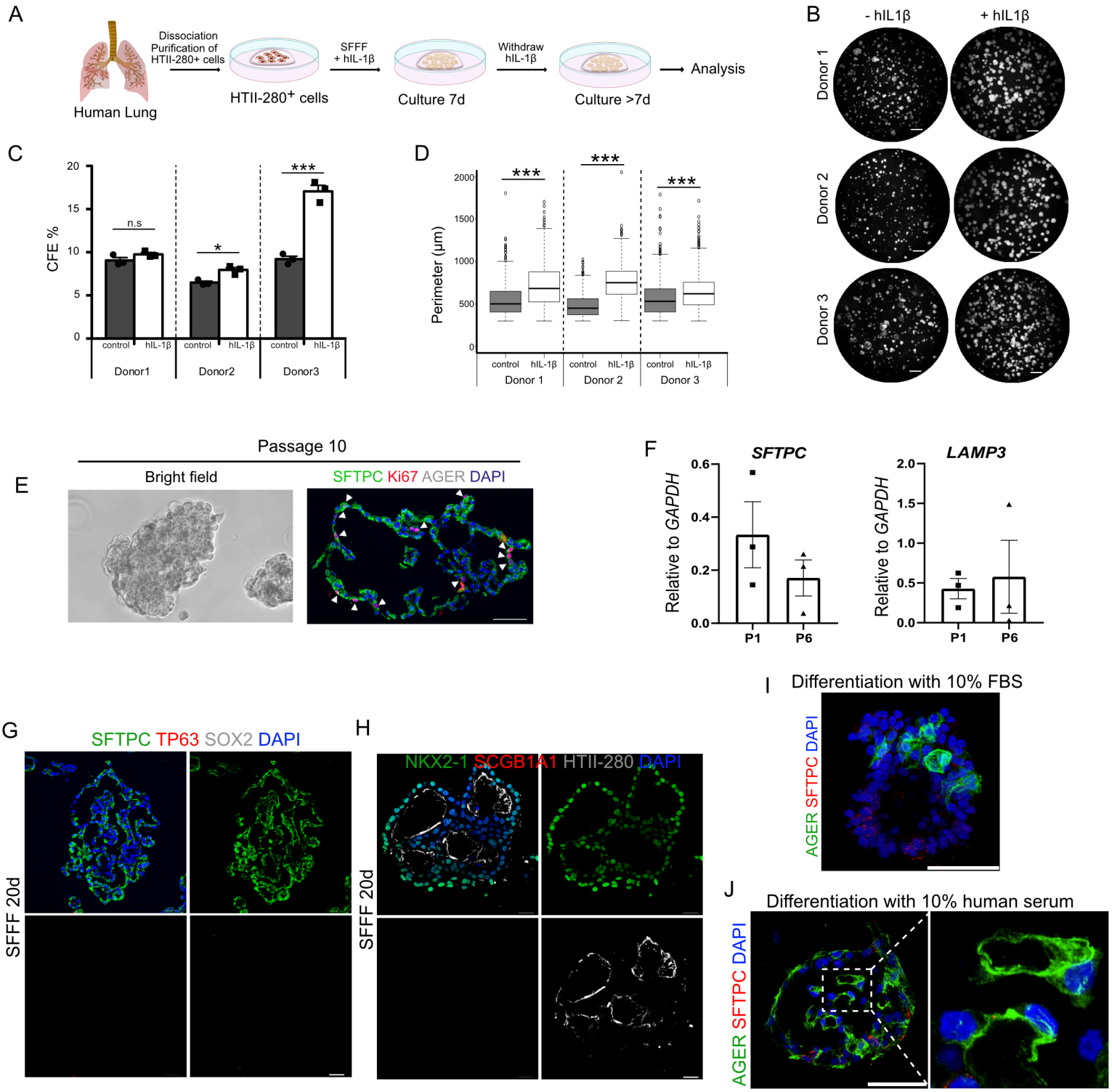

Fig. S3. Characterization of primary human alveolospheres. Related to Fig. 1.
A. Schematic of human alveolosphere culture in SFFF medium. hIL-1β was removed from medium at day 7 and cultured for an additional 7-15 days. B. Representative alveolosphere images of three individual donors at day 14. Quantification of colony formation efficiency (C) and size (perimeter) (D) of alveolospheres collected on day 14. E. Images of bright field (left) and immunostaining for SFTPC (green), Ki67 (red) and AGER (grey) in human alveolospheres at P10. F. Quantitative RT-PCR for *SFTPC* and *LAMP3* in human alveolospheres at P1 and P6. G. Immunostaining for SFTPC (green), and TP63 (red) and SOX2 (grey) on alveolosphere sections cultured in SFFF media for 20 days. H. Immunostaining for NKX2-1 (green), SCGB1A1 (red), and HTII-280 (white) on alveolosphere sections cultured in SFFF media for 20 days. I. Immunostaining for AGER (green) and SFTPC (red) in alveolospheres after induction of differentiation by 10% FBS for 10 days. J. Immunostaining for AGER (green) and SFTPC (red) on alveolospheres after induction of differentiation by human serum for 10 days. High magnification image (right) shows AGER$^+$ cells. Scale bars, 50 μm. Data are presented as mean s.e.m.

Figure S4

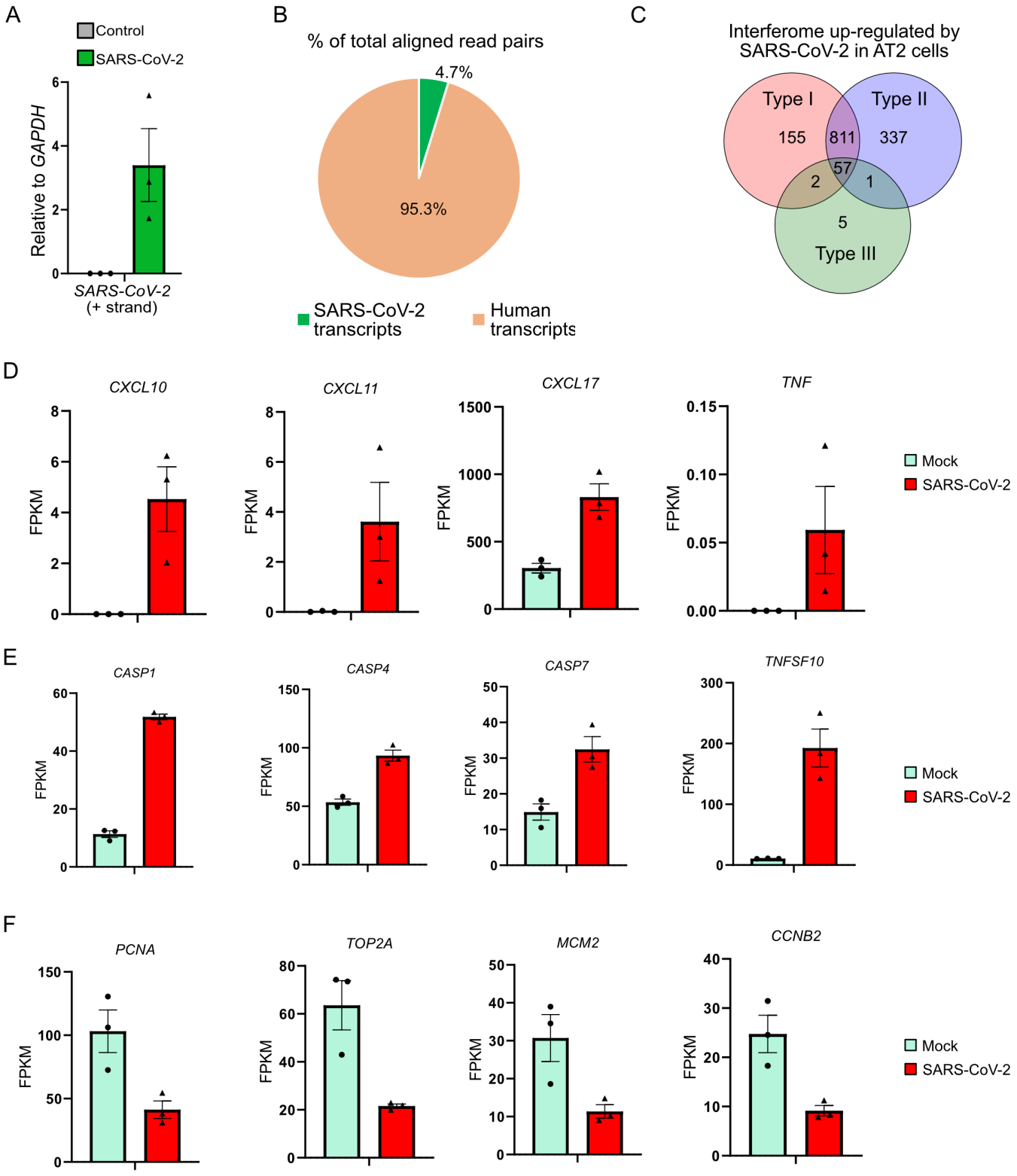

Fig. S4. SARS-CoV-2 infection activates interferon, inflammatory and cell death programs in AT2 alveolospheres. Related to Fig. 3.
A. Quantitative RT-PCR analysis for *SARS-CoV-2* transcripts in control and SARS-CoV-2 infected human AT2 alveolospheres. B. Percentage of aligned reads from human AT2 alveolospheres and SARS-CoV-2 in total bulk RNA-seq. C. Venn diagram shows enrichment analysis of IFN signaling pathways upregulated genes in SARS-CoV-2 infected human AT2 alveolospheres. Enrichment analysis was performed using Interferome. D-F. Expression levels of listed genes in control (green) and SARS-CoV-2 infected (red) AT2 alveolospheres detected by bulk RNA-seq. D-F show expression of cytokines/chemokines, cell death-related and proliferation-related genes, respectively. Data are presented as FPKM mean s.e.m.

Figure S5

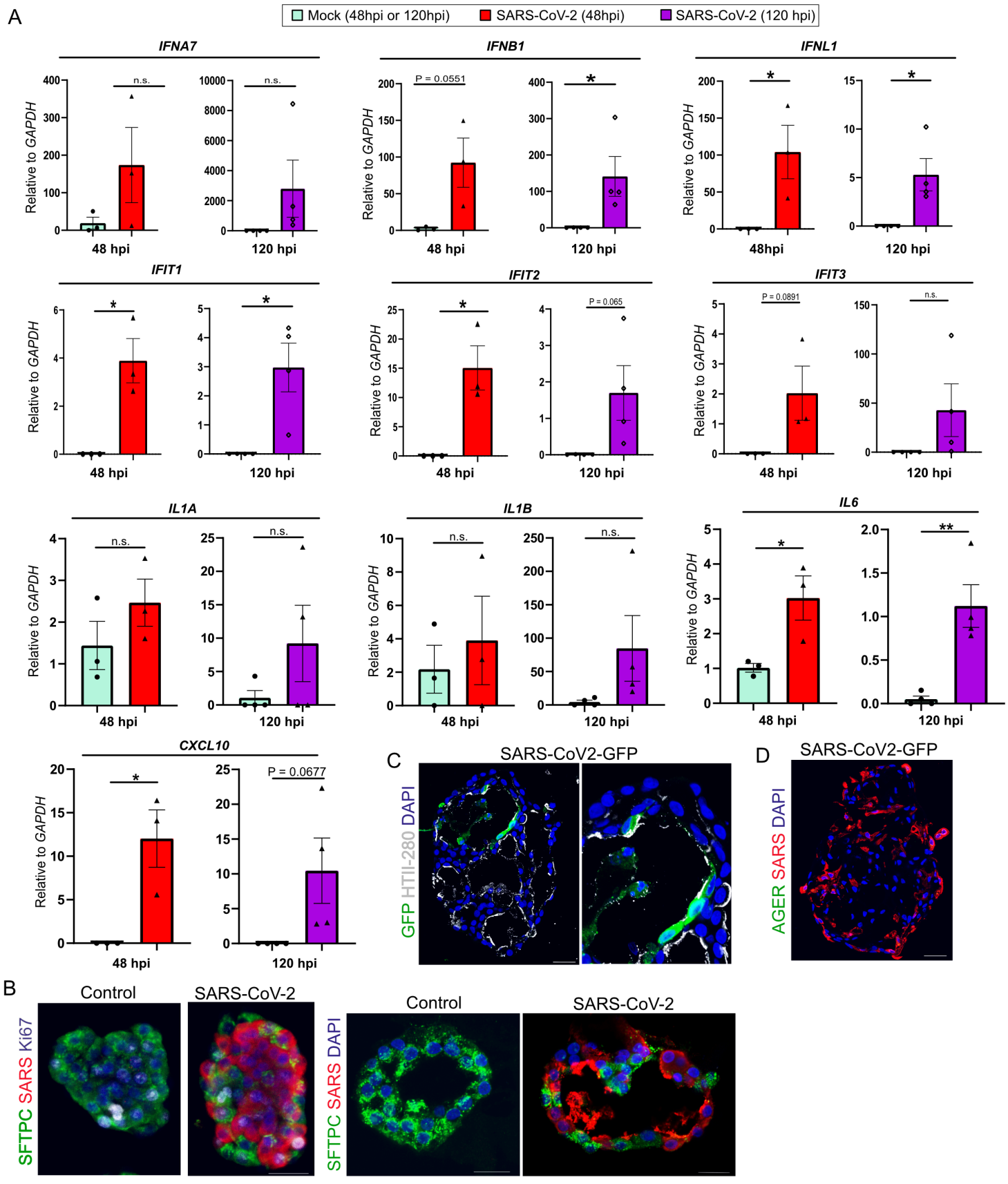

Fig. S5. Quantitative RT-PCR validated the upregulation of interferon targets in SARS-CoV-2 infected human AT2 alveolospheres. Related to Fig. 4.

A, IFN ligand, IFN-target and cytokine gene expression were measured by quantitative PCR in control (green) and SARS-CoV-2 infected human alveolospheres cultured in SFFF analyzed at 48h (red) and 120h (purple) after the virus infection. Data are presented as mean s.e.m. * and ** show $p < 0.05$ and $p < 0.01$, respectively. B. Immunostaining for SFTPC (green), SARS (red) and Ki67 (blue, left) and DAPI (blue, right) on SARS-CoV-2 infected human alveolospheres. C. Co-staining for GFP (green) and HTII-280 (grey) on SARS-CoV-2 infected alveolospheres. D. Co-immunostaining to detect SARS-CoV-2 (red) and AGER (green). Scale bars 30μm.

Figure S6

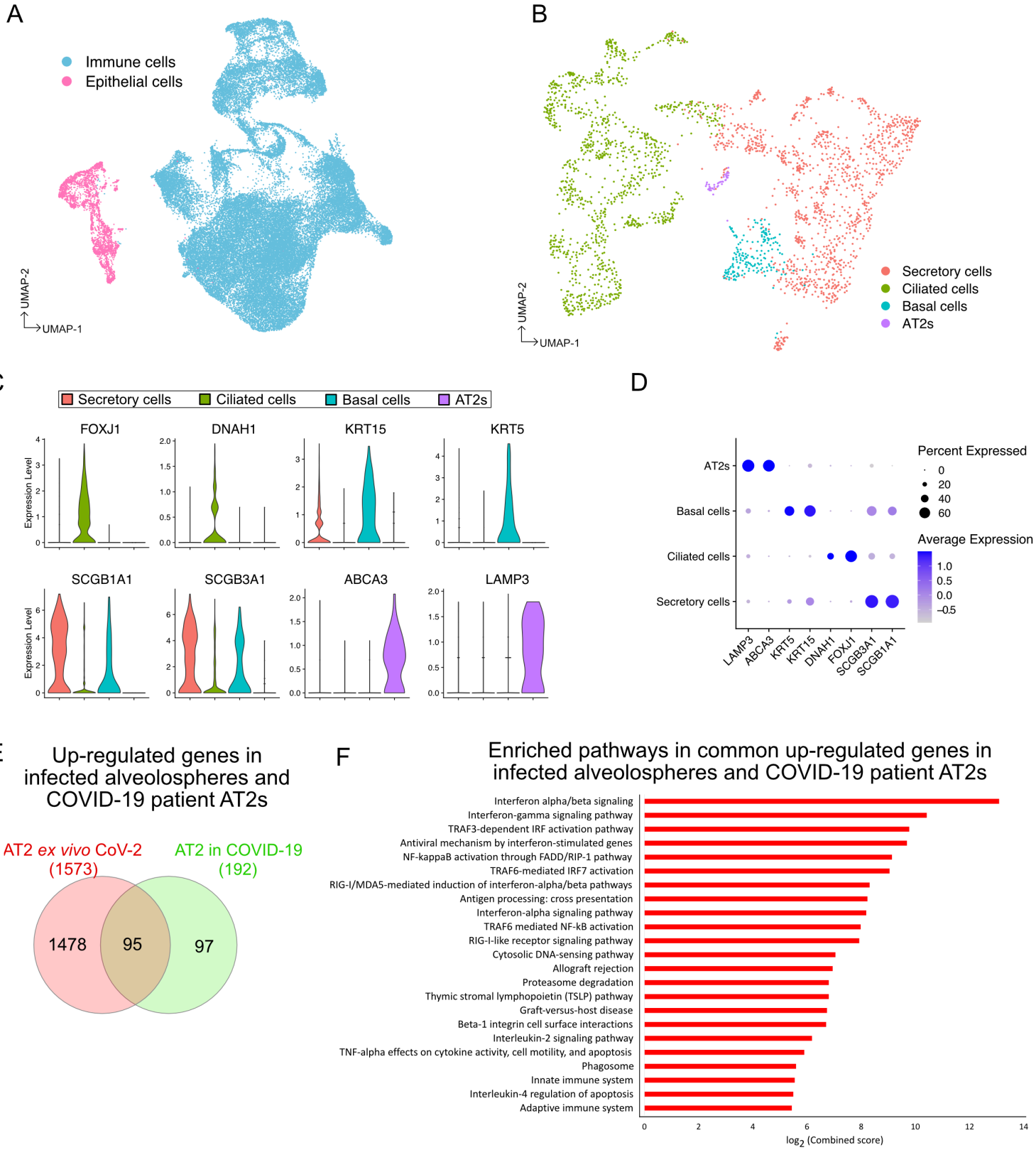

Fig. S6. Transcriptome-wide comparison of AT2s enriched transcripts in SARS-CoV-2 infected alveolospheres and COVID-19 lungs. Related to Fig. 5.

A. UMAP shows total cells containing epithelial cells (pink) and immune cells (blue) obtained from six severe-COVID-19 lung scRNA-seq data. B. UMAP shows total epithelial cells in severe COVID-19 patients. C. Violin plots show marker gene expression for secretory cells (red), ciliated cells (green), basal cells (blue), and AT2s (purple) in the epithelial cells obtained from the severe COVID-19 patient lungs. D. Dot plot shows cell type specific marker gene expression in epithelial cells obtained from the severe COVID-19 patients. E. Venn diagram shows overlapping genes upregulated in SARS-CoV-2 infected AT2 alveolospheres detected by Bulk RNA-seq (red) and AT2s isolated from COVID-19 patients detected by scRNA-seq (green). F. Pathway enrichment analysis in upregulated genes in AT2s from SARS-CoV-2 infected alveolospheres and COVID-19 patients. The scale shows $\log_2$ (combined score) obtained from BioPlanet database through Enrichr.

Figure S7

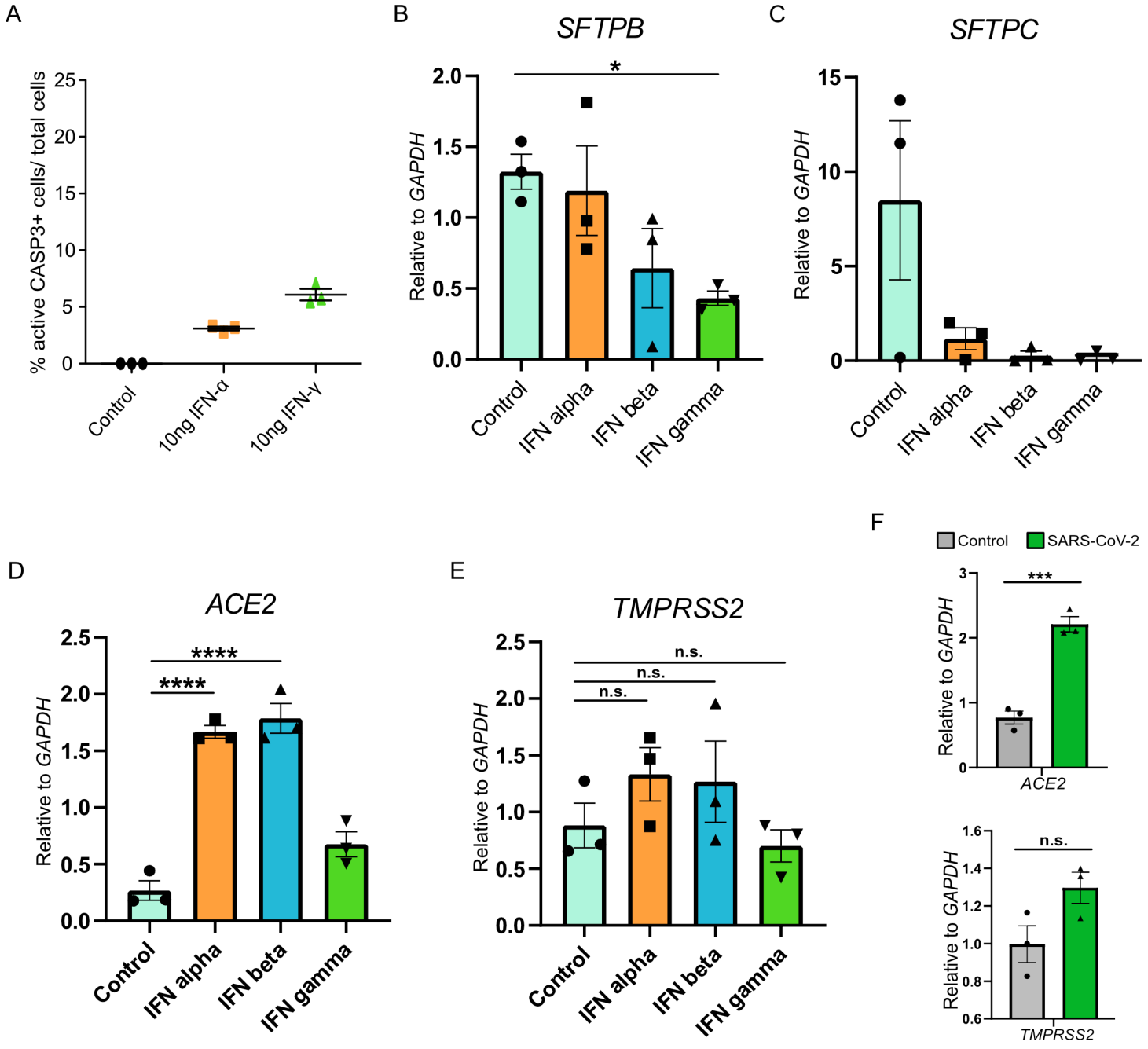

Fig. S7. Expression of *ACE2* and *TMPRSS2* in interferon and cytokines treated alveolospheres. Related to Fig. 6.

A. Quantification of active caspase3⁺ cells in total DAPI⁺ (per alveolosphere) cells in control and interferon treated human alveolospheres 72 hours post treatment. B-E. Quantitative RT-PCR analysis for *SFTPB* (B), *SFTPC* (C), *ACE2* (D), and *TMPRSS2* (E) in alveolospheres treated with interferons. F, Quantitative RT-PCR analysis for *ACE2* and *TMPRSS2* on control and SARS-CoV-2 infected (48h post infection) alveolospheres cultured in SFFF. Data are presented as mean s.e.m. *, ***, **** show $p < 0.05$, $p < 0.001$ and $p < 0.0001$, respectively.

	Component	SFFF concentration	AMM concentration	ADM concentration	Treatment period
Base medium	Advanced DMEM/F12				
Compounds	SB431542	10 μM	10 μM	-	all time
	CHIR99021	3 μM	3 μM	-	all time
	BIRB796	1 μM	1 μM	-	all time
	DMH-1	-	1 μM	-	all time
	Y-27632	10 μM	10 μM	-	0d-4d
Recombinant proteins	Human EGF	50 ng/ml	50 ng/ml	5 ng/ml	all time
	Mouse FGF10	10 ng/ml	10 ng/ml	1 ng/ml	all time
	Mouse IL-1β	10 ng/ml	10 ng/ml	-	First 4 days of culture
	Mouse Noggin	-	10 ng/ml	-	all time
Supplements	Heparin	5 μg/ml	5 μg/ml	5 μg/ml	all time
	B-27 supplement	1X	1X	1X	all time
	Antibiotic-Antimycotic	1X	1X	1X	all time
	HEPES	15 mM	15 mM	-	all time
	GlutaMAX	1X	1X	1X	all time
	N-Acetyl-L-Cysteine	1.25 mM	1.25 mM	1.25 mM	all time
	FBS	-	-	10%	all time

Table S1: Media composition (SFFF, AMM, and ADM) for human AT2 cells self-renewal or differentiation. **Related to STAR Methods**

	Component	Concentration SFFF	Concentration ADM	Treatment period
Base medium	Advanced DMEM/F12			
Compounds	SB431542	10 µM	-	all time
	CHIR99021	3 µM	-	all time
	BIRB796	1 µM	-	all time
	Y-27632	10 µM	-	0d-4d
Recombinant proteins	Human EGF	50 ng/ml	5 ng/ml	all time
	Human FGF10	10 ng/ml	1 ng/ml	all time
Supplements	Heparin	5 µg/ml	5 µg/ml	all time
	B-27 supplement	1X	1X	all time
	Antibiotic-Antimycotic	1X	1X	all time
	HEPES	15 mM	-	all time
	GlutaMAX	1X	1X	all time
	N-Acetyl-L-Cysteine	1.25 mM	1.25 mM	all time
	Human serum	-	10%	all time

Table S2: Media composition (SFFF and ADM) for human AT2 cells self-renewal or differentiation. **Related to STAR Methods**

Species	Gene	Sequence
Human	ACE2_Forward	ATCAGAGATCGGAAGAAGAAAAA
Human	ACE2_Reverse	TTGCTAATATCGATGGAGGCA
Human	TMPRSS2_Forward	CCGAGGAGAAAGGGAAGACC
Human	TMPRSS2_Reverse	TCACCCTGGCAAGAATCGAC
Human	SFTPB_Forward	CCATGATTCCCAAGGGTGCG
Human	SFTPB_Reverse	CAGCCATTCTCCTGTCGGC
Human	SFTPC_Forward	TCCAGAGAGCATCCCCAGTC
Human	SFTPC_Reverse	GGCTTCCACTGACCCTGC
Human	ABCA3_Forward	AGATGTAGCGGACGAGAGGA
Human	ABCA3_Reverse	GCTGCTCGTACACCTTGGAG
Human	LAMP3_Forward	AAGATGACCACTTTGGAAATGTG
Human	LAMP3_Reverse	GATGGCCCCAATCACAGGAA
Human	IFNA7_Forward	GGCCCGGTCCTTTTCTTTAC
Human	IFNA7_Reverse	ACTCCTCCTCTGGGAATCTGAA
Human	IFNB1_Forward	ACGCCGCATTGACCATCTA
Human	IFNB1_Reverse	TGGCCTTCAGGTAATGCAGA
Human	IFNL1_Forward	GGTGACTTTGGTGCTAGGC
Human	IFNL1_Reverse	AGTGACTCTTCCAAGGCG
Human	IFIT1_Forward	ATTTACAGCAACCATGAGTACAAA
Human	IFIT1_Reverse	TCCCACACTGTATTTGGTGTC
Human	IFIT2_Forward	TGCAACCATGAGTGAGAACA
Human	IFIT2__Reverse	GATAGGCCAGTAGGTTGCACA
Human	IFIT3_Forward	CAGAACTGCAGGGAAACAGC
Human	IFIT3_Reverse	GGAAGGATTTTCTCCAGGG
Human	CXCL10_Forward	AAGTGGCATTCAAGGAGTACC
Human	CXCL10_Reverse	ACGTGGACAAAATTGGCTTGC
Human	IL6_Forward	CTCCTTCTCCACAAGCGCC
Human	IL6_Reverse	GAAGGCAGCAGGCAACAC
Human	IL1A_Forward	TGAGTCAGCAAAGAAGTCAAG
Human	IL1A_Reverse	GGAGTGGGCCATAGCTTACA
Human	IL1B_Forward	TTCGAGGCACAAGGCACAA
Human	IL1B_Reverse	TGGCTGCTTCAGACACTTGAG
Human	GAPDH_Forward	TCGGAGTCAACGGATTTGG
Human	GAPDH_Reverse	TTCCCGTTCTCAGCCTTGAC
Mouse	Sftpc_Forward	ACAATCACCACCACAACGAG
Mouse	Sftpc_Reverse	AGCAAAGAGGTCCTGATGGA
Mouse	Abca3_Forward	CCGCCTCAGTTGTCAGCTTC
Mouse	Abca3_Reverse	ACATCACAGTGGAGGGATAGTG
Mouse	Lamp3_Forward	GCTTGGTGTTCCTTGGTGTTC
Mouse	Lamp3_Reverse	CCACTGTTGTGTGCTTGAGTC
Mouse	Gapdh_Forward	TTGAGGTCAATGAAGGGGTC
Mouse	Gapdh_Reverse	TCGTCCCGTAGACAAAATGG
SARS-CoV-2	N3_Forward	GGGAGCCTTGAATACACCAAA A
SARS-CoV-2	N3_Reverse	TGTAGCACGATTGCAGCATTG
SARS-CoV-2	Negative strand-specific RT primer	ACTGGAACACTAAACATAGCAGTGGTGTTA
SARS-CoV-2	Positive strand-specific RT primer	CCAAAGGCAATAGTGCGACCACCC
SARS-CoV-2	genome_1202-1363_Forward	AACCAAATGTGCCTTTCAACTC
SARS-CoV-2	genome_1202-1363_Reverse	AACAACAGCATTTTGGGGTAAG
SARS-CoV-2	genome_848-981_Forward	GGCTACCCTCTTGAGTGCATTA
SARS-CoV-2	genome_848-981_Reverse	GCAATTTCATGCTCATGTTCAC

Table S3. List of oligonucleotides used for quantitative RT-PCR. **Related to Fig. S5.**